Preprints of the 21st IFAC World Congress (Virtual)
Berlin, Germany, July 12-17, 2020

A Droop Approach for the Passivity–based Control of Microgrids ⋆

Isaac Ortega-Velázquez * **Sofía Avila-Becerril** *
Gerardo Espinosa-Pérez *

* *Universidad Nacional Autónoma de México, Facultad de Ingeniería-UNAM 04510 Ciudad de México, México*

Abstract: In this paper, the stability properties of a microgrid in closed-loop with local inverters' controllers and a droop power-sharing scheme are studied. The main result is the formal statement that this system is asymptotically stable concerning the equilibrium point that satisfies desired operating conditions. In contrast to the results reported in the literature, neither the stability analysis of the inverter's dynamics is omitted, nor is it assumed that the only dynamic behavior is that corresponding to the droop scheme. The contribution exploits the inclusion of a passivity–based control law for the inverters and the input–to–state stability properties exhibited by the considered droop algorithm. The validity of the analysis is illustrated via a numerical evaluation.

Keywords: Microgrids, passivity–based control, droop control.

1. INTRODUCTION

The benefit obtained by the inclusion of microgrids (MGs) for electric power generation is a well-recognized fact. The challenges that impose their proper operation, however, still require the attention of the scientific community (Rojas and Rousan [2017], Tuffner et al. [2018], Rajesh et al. [2017]). The main objective of a MG is two–fold: voltage regulation in all the nodes and fulfillment of the demanded power by the loads. This task must be carried out taking into account the intermittency of the available energy, the necessity of conditioning the generated energy, and the sensitivity of the devices involved to sudden changes in the network operation, among other problems.

To deal with the problem, it is necessary to first locally regulate the voltages and currents of the generation units for later on implementing power-sharing algorithms that consider the amount of power that each source can provide (Agundis-Tinajero et al. [2019], Barklund et al. [2008]). In fact, if each source is equipped with an inverter, the local controls are conceived to divide the sources into two types: grid–forming inverters, with the main objective of regulating the voltages nodes and grid–following inverters, that provide the maximum amount of power that they are capable of generating (See Han et al. [2016], Pedrasa and Spooner [2006]). Many solutions have been reported. The most relevant are related to the use of classical proportional integral (PI) techniques for the local controls and the droop control for the power-sharing step (Han et al. [2016], Rocabert et al. [2012], Lopes et al. [2006], Guerrero et al. [2013]). In this context, the implementation of the PI schemes is carried out without giving formal proof to justify stability properties, while for the droop algorithm (for example in Zhong and Hornik [2012]) several quite important analyses of its stability properties have been provided, although all of them are stated without considering the dynamics of the local controls (Schiffer et al. [2014], Simpson-Porco et al. [2013]).

In this paper, the stability study of a MG model that explicitly includes both the inverter dynamic and the droop algorithm is approached. The result considers the design of the local controllers as a continuation of the work developed by the authors in a series of publications (Avila-Becerril et al. [2018, 2017]) and the droop control algorithm reported in Konstantopoulos et al. [2015] because the dynamic behavior of this version tends to the behavior of the basic droop algorithm and exhibits some input–to–state stability (ISS) properties that are fundamental in obtaining the main contribution of the paper.

The system approached in this paper considers the existence of grid–forming and grid–following inverters. Thus, a passivity-based control (PBC) scheme is proposed to guarantee the regulation of the output voltage of the grid–forming inverters, while the voltages and currents of the grid–following devices are steered to values that correspond to the maximum amount of power that can be extracted from them. In addition, the grid–forming sources are provided with the droop scheme which, depending on the power demanded by the loads, generates the voltage reference required to implement the local control law. Interestingly enough, the final structure of the controlled system satisfies the practical requirements for using only local variables measurements'. Concerning the formal mathematical analysis, the Hamiltonian structure of the closed loop is exploited in the analysis since it exhibits some passivity and ISS properties that, in conjunction with the ISS properties of the droop scheme, allow to establishing asymptotic stability properties of the equilibrium point.

The rest of the paper is organized as follows: In Section 2 the model considered for the inverters is presented while

⋆ Part of this work was supported by DGAPA–UNAM under PAPIIT grants IN118019 –IA103519. Isaac Ortega-Velázquez (isaacbike8@comunidad.unam.mx)

the PBC design is included in Section 3. Section 4, is devoted to introducing the structure of Droop control, and the main result of the paper the stability proof for the whole closed–loop system is stated in Section 5. The numerical evaluation is contained in Section 6, and some concluding remarks are presented in Section 7.

2. INVERTERS MODELING

Each distributed energy resource (DER) includes a DC voltage (or current) source, power semiconductor devices, and an LC filter for approximately obtaining a sinusoidal output voltage. Since there are two types of DC sources, it is convenient to split the set of inverters into two subsets, i.e. $\mathcal{N} = \mathcal{N}_1 \cup \mathcal{N}_2$, such that $\mathcal{N}_1$ contains grid-forming nodes and $\mathcal{N}_2$ corresponds to grid-following nodes.

Grid-forming inverters Consider a generic voltage–fed inverter located at the $i-$th node of an MG, i.e. $i \in \mathcal{N}_1$, represented in Fig. 1 where $V_{0,i} > 0 \in \mathbb{R}$, $u_{\nu,i} \in \mathbb{R}$ is the modulation (control) signal, while $L_{\nu,i}$, $C_{\nu,i}$ are the strictly positive parameters of the output filter. Each grid-forming inverter is subject to a current demand denoted by $I_{L\nu,i}$. Denote the inverter's output voltage by $v_{\nu,i}$, the

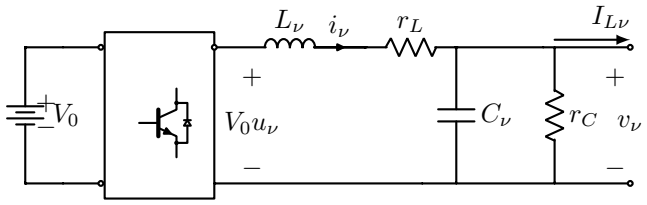

Fig. 1. Voltage-fed inverter scheme

inductor's current by $i_{\nu,i}$ and assume linear constitutive relationships for both the inductor and the capacitor. If the $|\mathcal{N}_1|$ individual sources are piled up, then it is immediately obtained that the dynamic model in compact form is given by

$$L_\nu \frac{d}{dt} i_\nu = -r_L i_\nu - v_\nu + V_0 u_\nu, \tag{1a}$$

$$C_\nu \frac{d}{dt} v_\nu = -r_C^{-1} v_\nu + i_\nu - I_{L\nu}, \tag{1b}$$

with the vectors $i_\nu = col\{i_{\nu,i}\}$, $v_\nu = col\{v_{\nu,i}\}$, $u_\nu = col\{u_{\nu,i}\}$, $I_{L\nu} = col\{I_{L\nu,i}\} \in \mathbb{R}^{|\mathcal{N}_1|}$, the parameter matrices $L_\nu = diag\{L_{\nu,i}\}$, $C_v = diag\{C_{\nu,i}\}$, $r_L = diag\{r_{L,i}\}$, $r_C = diag\{r_{C,i}\} \in \mathbb{R}^{|\mathcal{N}_1|\times|\mathcal{N}_1|}$, and the matrix $V_0 = diag\{V_{0,i}\} \in \mathbb{R}^{|\mathcal{N}_1|\times|\mathcal{N}_1|}$. Moreover, by defining the state

$$x_\nu := [i_\nu^\top \quad v_\nu^\top]^\top \in \mathbb{R}^{2|\mathcal{N}_1|} \tag{2}$$

and by recognizing the total stored energy function for these devices $W_v : \mathbb{R}^{2|\mathcal{N}_1|} \times \mathbb{R}^{2|\mathcal{N}_1|} \to \mathbb{R}_{\geq 0}$ as

$$W_v(x_\nu) = \frac{1}{2} x_\nu^\top P_\nu x_\nu, \tag{3}$$

with $P_\nu = diag\{L_\nu, C_\nu\} > 0$, model (1) can then be equivalently written as a Hamiltonian system of the form

$$P_\nu \dot{x}_\nu = (J_\nu - R_\nu) x_\nu + G_\nu u_\nu - \begin{bmatrix} 0 \\ I_{L\nu} \end{bmatrix}, \tag{4}$$

where $R_\nu = diag\{r_L, r_C^{-1}\} > 0$,

$$J_\nu = \begin{bmatrix} 0 & -\mathbf{I} \\ \mathbf{I} & 0 \end{bmatrix} = -J_\nu^\top, \text{ and } G_\nu = \begin{bmatrix} V_0 \\ 0 \end{bmatrix} \in \mathbb{R}^{2|\mathcal{N}_1|\times|\mathcal{N}_1|}$$

Grid-following inverters A generic grid-following inverter located at the $i-$th node of a MG such that $i \in \mathcal{N}_2$, is represented in Fig. 2 where $I_{0,i} > 0 \in \mathbb{R}$, $u_{\kappa,i} \in \mathbb{R}$ is the modulation (control) signal, while $L_{\kappa,i}$, $C_{DC,i}$, $r_{\kappa_L,i}$, and $r_{DC,i} \in \mathbb{R}$ are strictly positive parameters of the output filter. Now consider $|\mathcal{N}_2|$ current–fed inverters, denote the

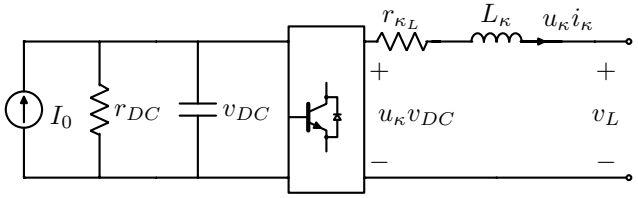

Fig. 2. Current-fed inverter scheme

inverter's output voltage by $v_{L,i}$, the capacitor's voltage in the DC side by $v_{DC,i}$, while $i_{\kappa,i}$ is the inductor's current, and linear inductors and capacitors, then the model in vector notation is given by

$$L_\kappa \frac{d}{dt} i_\kappa = -r_{\kappa_L} i_\kappa + U_\kappa v_{DC} - v_L, \tag{5a}$$

$$C_{DC} \frac{d}{dt} v_{DC} = -r_{DC}^{-1} v_{DC} - U_\kappa i_\kappa + I_0, \tag{5b}$$

with the vectors $i_\kappa = col\{i_{\kappa,i}\}$, $v_{DC} = col\{v_{DC,i}\} \in \mathbb{R}^{|\mathcal{N}_2|}$, the matrix $U_\kappa = diag\{u_{\kappa,i}\} \in \mathbb{R}^{|\mathcal{N}_2|\times|\mathcal{N}_2|}$, the parameter matrices $L_\kappa = diag\{L_{\kappa,i}\}$, $C_{DC} = diag\{C_{DC,i}\}$, $r_{\kappa_L} = diag\{r_{\kappa_L,i}\}$, $r_{DC} = diag\{r_{DC,i}\} \in \mathbb{R}^{|\mathcal{N}_2|\times|\mathcal{N}_2|}$, and the vectors $v_L = col\{v_{L,i}\}$, $I_0 = col\{I_{0,i}\} \in \mathbb{R}^{|\mathcal{N}_2|}$. Define the state

$$x_\kappa := [i_\kappa^\top \quad v_{DC}^\top]^\top \in \mathbb{R}^{2|\mathcal{N}_2|} \tag{6}$$

and the total stored energy function $W_\kappa : \mathbb{R}^{2|\mathcal{N}_2|} \times \mathbb{R}^{2|\mathcal{N}_2|} \to \mathbb{R}_{\geq 0}$ by

$$W_\kappa(x_\kappa) = \frac{1}{2} x_\kappa^\top P_\kappa x_\kappa, \tag{7}$$

with the parameters matrix $P_\kappa = diag\{L_\kappa, C_{DC}\}$. Thus, model (5) can be equivalently written as a PCH system of the form

$$P_\kappa \dot{x}_\kappa = (J_\kappa(U_\kappa) - R_\kappa) x_\kappa + e_\kappa, \tag{8}$$

with $R_\kappa = diag\{r_{\kappa_L}, r_{DC}^{-1}\}$ and the matrices

$$J_\kappa(U_\kappa) = \begin{bmatrix} 0 & U_\kappa \\ -U_\kappa & 0 \end{bmatrix} = -J_\kappa^\top(U_\kappa), \text{ and } e_\kappa = \begin{bmatrix} -v_L \\ I_0 \end{bmatrix}.$$

Remark 1. An important property enjoyed by the previous model is that with an appropriate definition of the skew-symmetric J_i, matrix $J_\kappa(U_k)$ can be rewritten as

$$J_\kappa(U_k) = \sum_{i=1}^{|\mathcal{N}_2|} J_i u_{\kappa,i}. \tag{9}$$

As a consequence, model (8) can also be expressed as

$$P_\kappa \dot{x}_\kappa = -R_\kappa x_\kappa + G_\kappa(x_\kappa) u_k + e_\kappa, \tag{10}$$

with the control input $u_k = col\{u_{\kappa,i}\} \in \mathbb{R}^{|\mathcal{N}_2|}$ and

$$G_\kappa(x_\kappa) := \left[J_1 x_\kappa \vdots \cdots \vdots J_{|\mathcal{N}_2|} x_\kappa \right] \in^{2|N_2|\times|N_2|}. \tag{11}$$

3. PASSIVITY–BASED CONTROLLER DESIGN

In this section, following the ideas reported in Cisneros et al. [2015] and Avila-Becerril et al. [2018], we present

the inverters' controllers that steer the output currents and voltages of the inverters to a desired state.

Before we formulate the control problem, we first identify the admissible voltages and currents that the inverters are able to follow. These trajectories $x_\nu^\star := [i_\nu^{\star\top} \quad v_\nu^{\star\top}]^\top \in \mathbb{R}^{2|\mathcal{N}_1|}$ and $x_\kappa^\star := [i_\kappa^{\star\top} \quad v_{DC}^{\star\top}]^\top \in \mathbb{R}^{2|\mathcal{N}_2|}$ verify that

$$P_\nu \dot{x}_\nu^\star = (J_\nu - R_\nu)x_\nu^\star + G_\nu u_\nu^\star - \begin{bmatrix} 0 \\ I_{L\nu} \end{bmatrix}, \tag{12a}$$

$$P_\kappa \dot{x}_\kappa^\star = (J_\kappa(U_\kappa^\star) - R_\kappa)x_\kappa^\star + e_\kappa, \tag{12b}$$

for some $u_\nu^\star$, $u_\kappa^\star$ and for the measured current $I_{L\nu}$ as well as the measured voltage v_L.

It is important to notice that in the case of the grid-forming inverters for a given $u_\nu^\star$ the corresponding $x_\nu^\star$ is determined by the solution of (12a). Section 4 is dedicated to obtaining $u_\nu^\star$. On the other hand, since the system (12b) is related to the grid-following nodes, the output reference currents $i_\kappa^\star$ are assumed known. Given $i_\kappa^\star$, the i–th entry of $u_{\kappa,i}^\star$ is given by

$$u_{\kappa,i}^\star = \frac{1}{\|x_{\kappa,i}^\star\|^2} \left(x_{\kappa,i}^\star\right)^T J_i^T \left[P_{\kappa,i}\dot{x}_{\kappa,i}^\star + R_{\kappa,i}x_{\kappa,i}^\star - Q_i\right], \tag{13}$$

with

$$J_i = \begin{bmatrix} 0 & 1 \\ -1 & 0 \end{bmatrix}, \; Q_i = \begin{bmatrix} v_{L,i} \\ I_{0,i} \end{bmatrix},$$

and $v_{DC,i}^\star$ obtained as the solution of

$$\begin{aligned} C_{DC,i}\dot{v}_{DC,i}^\star = &-\frac{i_{\kappa,i}^\star}{v_{DC,i}^\star}\left[L_{\kappa,i}\dot{i}_{\kappa,i}^\star + r_{\kappa,i}i_{\kappa,i}^\star + v_{L,i}\right] \\ &- r_{DC,i}^{-1}v_{DC,i}^\star + I_{0i}, \end{aligned} \tag{14}$$

considering $v_{DC,i}^\star(0) > 0$.

Remark 2. Equations (13) and (14) are singularity-free, and their solutions tend to a (in average) positive value since its structure is equivalent to

$$\frac{1}{2}C_{DC,i}\dot{w} = -i_{\kappa,i}^\star\left[L_{\kappa,i}\dot{i}_{\kappa,i}^\star + r_{\kappa,i}i_{\kappa,i}^\star + v_{L,i}\right] - r_{DC,i}^{-1}w + I_{0i}w^{\frac{1}{2}}$$

where $w = (v_{DC,i}^\star)^2$, avoiding any singular behavior as long as $v_{DC,i}^\star(0) > 0$. This can be proven following arguments as those presented in Sandoval et al. [2012].

3.1 Inner Controllers

We now assume that the desired output currents and voltages of the inverters are admissible trajectories that fulfill the following:

- **A.1** The reference state $x_\nu^\star$ corresponds to a given active power load sharing among the grid-forming inverters.
- **A.2** An external controller provides the bounded reference signal $i_\kappa^\star$.

For presenting the controllers, we first introduce the error variables $\tilde{x}_\nu = x_\nu - x_\nu^\star$ and $\tilde{x}_\kappa = x_\kappa - x_\kappa^\star$. These variables have a dynamic represented by

$$P_\nu \dot{\tilde{x}}_\nu = (J_\nu - R_\nu)\tilde{x}_\nu + G_\nu \tilde{u}_\nu, \tag{15a}$$

$$P_\kappa \dot{\tilde{x}}_\kappa = (J_\kappa(\tilde{U}_\kappa) - R_\kappa)\tilde{x}_\kappa, \tag{15b}$$

with $\tilde{u}_\nu := u_\nu - u_\nu^\star$ and $\tilde{U}_\kappa := U_\kappa - U_\kappa^\star$. The control objective is formulated as to design control inputs u_ν and u_κ such that

$$\lim_{t\to\infty} \tilde{x}_\nu = 0, \quad \lim_{t\to\infty} \tilde{x}_\kappa = 0, \tag{16}$$

guaranteeing internal stability.

Proposition 3. Consider the MG model (4)–(8) under **A.1**-**A.2** and assume the following:

- **A.3** The demanded current and voltage $I_{L\nu}$ and v_L are known bounded continuous functions.
- **A.4** The prescribed input voltage $u_\nu^\star$ is a known bounded function with bounded first derivative.
- **A.5** The reference $v_\nu^\star$ is a known bounded function with bounded first derivative.
- **A.6** All the inverters' parameters are positive and known. The input voltages V_0 and currents I_0 are also known.

Under these conditions, the control law given by

$$u_\nu = V_0^{-1}(-K_{p\nu}\tilde{i}_\nu + K_{i\nu}y_\nu) + u_\nu^\star, \tag{17a}$$

$$\dot{y}_\nu = -\tilde{i}_\nu, \tag{17b}$$

$$u_\kappa = -K_{p\kappa}G_\kappa^\top(x_\kappa^\star)\tilde{x}_\kappa + K_{i\kappa}y_\kappa + u_\kappa^\star, \tag{17c}$$

$$\dot{y}_\kappa = -G_\kappa^\top(x_\kappa^\star)\tilde{x}_\kappa, \tag{17d}$$

with $u_\nu^\star$ and $u_\kappa^\star$ satisfying (12), and the gain matrices $K_{p\nu}, K_{i\nu} \in \mathbb{R}^{|\mathcal{N}_1|\times|\mathcal{N}_1|} > 0$ and $K_{p\kappa}, K_{i\kappa} \in \mathbb{R}^{|\mathcal{N}_2|\times|\mathcal{N}_2|} > 0$ achieve the control objective (16) guaranteeing internal stability.

Proof. To prove the stability of the equilibrium $\tilde{x}_\nu = \tilde{x}_\kappa = 0$, we take the time derivative of

$$\begin{aligned} H_\nu(\tilde{x}_\nu, y_\nu, \tilde{x}_\kappa, y_\kappa) = \frac{1}{2}\big(&\tilde{x}_\nu^\top P_\nu \tilde{x}_\nu + y_\nu^\top K_{i\nu}y_\nu \\ &+ \tilde{x}_\kappa^\top P_\kappa \tilde{x}_\kappa + y_\kappa^\top K_{i\kappa}y_\kappa\big) \end{aligned} \tag{18}$$

along the trajectories of the system (15) in closed-loop with (17), which gives

$$\begin{aligned} \dot{H}_\nu &= -\tilde{x}_\nu^\top \bar{R}_\nu \tilde{x}_\nu - \tilde{x}_\kappa^\top R_\kappa \tilde{x}_\kappa - \tilde{x}_\kappa^\top G_\kappa(x_\kappa^\star)K_{p\kappa}G_\kappa^\top(x_\kappa^\star)\tilde{x}_\kappa \\ &\le -\lambda_{\min}\left\{\bar{R}_\nu\right\}\|\tilde{x}_\nu\|^2 - \lambda_{\min}\left\{R_\kappa\right\}\|\tilde{x}_\kappa\|^2 \\ &\quad - \lambda_{\min}\left\{K_{p\kappa}\right\}\|G_\kappa^\top(x_\kappa^\star)\tilde{x}_\nu\|^2 < 0, \end{aligned}$$

with $\bar{R}_\nu = diag\{r_L + K_{p\nu}, r_C^{-1}\}$. Finally, following similar arguments to those of Cisneros et al. [2015], we can conclude global asymptotic stability of $\tilde{x}_\nu = \tilde{x}_\kappa = 0$.

For the grid-forming inverters, the internal stability comes from **A.4-A.5**, and in Section 5 we will investigate this issue. In the case of the grid-following inverters, we use **A.3**, **A.6**, and input-to-state properties. For this, we take the admissible trajectories $x_\kappa^\star := [i_\kappa^{\star\top} \quad v_{DC}^{\star\top}]^\top \in \mathbb{R}^{2|\mathcal{N}_2|}$ solutions of (12b) and the Lyapunov function

$$W_\kappa(x_\kappa^\star) = \frac{1}{2}x_\kappa^{\star\top}P_\kappa x_\kappa^\star, \tag{19}$$

that has a time derivative along the trajectories (12b) as

$$\begin{aligned} \dot{W}_\kappa &= -x_\kappa^{\star\top}R_\kappa x_\kappa^\star + x_\kappa^{\star\top}e_\kappa \\ &\le -(1-\theta_\kappa)\lambda_{\min}\{R_\kappa\}\|x_\kappa^\star\|^2 \\ &\forall \;\; \|x_\kappa^\star\| \ge \frac{\|e_\kappa\|}{\theta_\kappa\lambda_{\min}\{R_\kappa\}} > 0, \end{aligned} \tag{20}$$

for $0 \le \theta_\kappa \le 1$ and e_κ defined in (8). Inequality (20) implies that system (12b) is ISS such that

$$\|x_\kappa^\star\| \le \gamma_\kappa(\|e_\kappa\|) + \beta_\kappa. \tag{21}$$

Finally, from **A.3** and **A.6**, $e_\kappa \in \mathcal{L}_\infty$, which concludes the proof.

4. DROOP CONTROL

To ensure that Assumption **A.1** is satisfied, it is necessary to generate appropriate references. To solve this problem, in this paper a droop control scheme is adopted.

Unlike the reported in the literature, we use a robust droop control to generate the $i-th$ voltage reference for the inner controllers of the grid-forming nodes, which are denoted by $V_{0,i}u^\star_{\nu,i}$. We assume that these references are sinusoidal with phase angle $\theta_{\nu,i}$ and amplitude $\sqrt{2}E_{\nu,i}$, *i.e.*,

$$V_{0,i}u^\star_{\nu,i} = \sqrt{2}E_{\nu,i}\sin(\theta_{\nu,i}). \tag{22}$$

In the next subsection, we introduce the robust droop controller to generate the signal $y_{droop,i}$ that provides the magnitudes and angles of the sinusoidal references (22).

Inspired by Konstantopoulos et al. [2015], the robust droop controller is implemented in the following form:

$$y_{droop,i} = \sqrt{2}E_i z_i, \tag{23}$$

where the dynamics of the RMS voltage E_i and the phase angle θ_i of the $i-th$ inverters are given by

$$\begin{bmatrix}\dot{E}_i\\ \dot{E}_{qi}\end{bmatrix} = \begin{bmatrix}-R_E & \dot{\phi}_i\\ -\dot{\phi}_i & -R_E\end{bmatrix}\begin{bmatrix}E_i\\ E_{qi}\end{bmatrix}, \tag{24a}$$

$$\begin{bmatrix}\dot{z}_i\\ \dot{z}_{qi}\end{bmatrix} = \begin{bmatrix}-R_z & \dot{\theta}_i\\ -\dot{\theta}_i & -R_z\end{bmatrix}\begin{bmatrix}z_i\\ z_{qi}\end{bmatrix}, \tag{24b}$$

where

$$\dot{\phi}_i = \left(K_e(E_{\text{ref}} - V_i^\star) - n_i Q_i^\star\right)c, \tag{25a}$$

$$\dot{\theta}_i = \left(\omega_{\text{ref}} - m_i P_i^\star\right), \tag{25b}$$

$$R_E = k_E(E_i^2 + E_{qi}^2 - V_i^2), \tag{25c}$$

$$R_z = k_z(z_i^2 + z_{qi}^2 - 1), \tag{25d}$$

with E_{ref} and ω_{ref} as the rated voltage and angular frequency, respectively. Furthermore, $c \in \mathbb{R}$ is a positive constant, while $V_i^\star$ in (25a) represents the RMS output voltage of the grid-forming inverters such that

$$V_i^\star := \sqrt{\frac{1}{T}\int_{t_0}^{t_0+T} v_{\nu,i}^{\star 2}dt}.$$

Similarly, $P_i^\star$ and $Q_i^\star$ are the active and reactive power calculated as functions of $(v^\star_{\nu,i}, i^\star_{\nu,i})$. The control parameters K_e, n_i and $m_i \in \mathbb{R}$ are determined by the droop ratio (Zhong and Hornik [2012]), while k_E, k_z, and V_i are positive constants.

Finally, we get the reference of the inner controller by matching (23) with (22). In Konstantopoulos et al. [2015] it is proven that the solution of (24) converges to the solution of the conventional robust droop controller (Zhong and Hornik [2012]). This fact makes **A.1** feasible.

5. CLOSED–LOOP STABILITY ANALYSIS

In this section the main result of the paper is presented: the stability analysis of the whole closed–loop system composed of the PBC introduced in Section 3 and the droop control presented in Section 4. To this end, we first establish ISS properties of the individual systems to then establish that an interconnection as illustrated in Fig. 3 ensures ISS properties from $I_{L\nu}$ to $x^\star_\nu$. Specifically, we show that if **A.3** holds and we use the droop control to generate $V_0u^\star_\nu$, then the references $x^\star_\nu$ remain bounded.

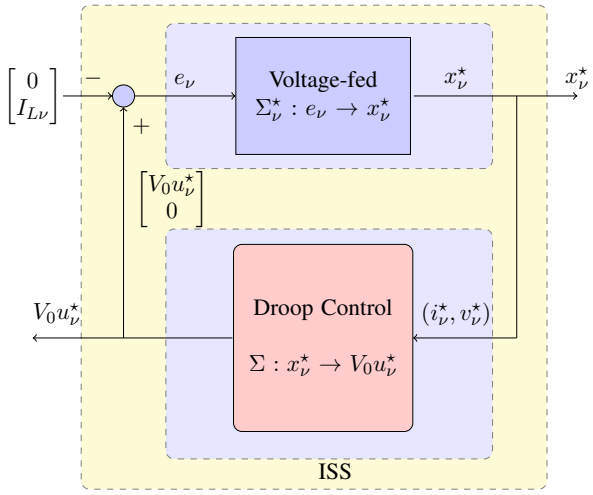

Fig. 3. Interconnection with droop control

Voltage-fed inverters We first consider the admissible trajectories $x^\star_\nu := [i^{\star\top}_\nu \quad v^{\star\top}_\nu]^\top \in \mathbb{R}^{2n}$, which are solutions of (12a) and the Lyapunov function $W_\nu(x^\star_\nu)$

$$W_\nu(x^\star_\nu) = \frac{1}{2}x^{\star\top}_\nu P_\nu x^\star_\nu. \tag{26}$$

Define

$$e_\nu = \begin{bmatrix}V_0u^\star_\nu\\ -I_{L\nu}\end{bmatrix} \tag{27}$$

such that the time derivative of W_ν along (12a) is

$$\begin{aligned}\dot{W}_\nu &= -x^{\star\top}_\nu R_\nu x^\star_\nu + x^{\star\top}_\nu e_\nu\\ &\le -(1-\theta_\nu)\lambda_{\min}\{R_\nu\}\|x^\star_\nu\|^2\\ &\forall\ \|x^\star_\nu\| \ge \frac{\|e_\nu\|}{\theta_\nu\lambda_{\min}\{R_\nu\}} > 0\end{aligned} \tag{28}$$

and $0 \le \theta_\nu \le 1$. Inequality (28) implies that system (12a) is input-to-state stable (Khalil [1996]) such that

$$\|x^\star_\nu\| \le \gamma_\nu(\|e_\nu\|) + \beta_\nu, \tag{29}$$

where

$$\gamma_\nu = \sqrt{\frac{\lambda_{\max}\{P_\nu\}\|e_\nu\|^2}{\lambda_{\min}\{P_\nu\}\ \theta_\nu^2\ \lambda^2_{\min}\{R_\nu\}}}.$$

Droop control First, notice that the droop controller (24) has as an input a pair of currents and voltages as shown in Fig. 3. This input is denoted by

$$e_{droop} = \begin{bmatrix}i^\star_{\nu,i}\\ v^\star_{\nu,i}\end{bmatrix}. \tag{30}$$

According to Konstantopoulos et al. [2015], since E_i, E_{qi} are bounded in $[-V_i, V_i]$ and z_i, z_{qi} are bounded in $[-1, 1]$ for any input e_{droop}, then

$$\|y_{droop,i}\| = \sqrt{2}\,\|\,E_i z_i\,\| \le \beta_{droop}. \tag{31}$$

The controller (24) is also finite gain $\mathcal{L}_\infty$ stable with gain $\gamma_{droop} = 0$, since (31) holds true independently of the input e_{droop}.

Interconnection On the one hand, inequality (31) means that for the grid-forming inverters the voltage $V_0u^\star_\nu$ in (12a) can be bounded by

$$\|V_0u^\star_\nu\| \le \beta_{droop}. \tag{32}$$

Notice from (27) (see also Fig. 3) and the triangle inequality that

$$\|e_\nu\| \leq \|I_{L\nu}\| + \beta_{droop}. \tag{33}$$

Using the ISS properties of the voltage-fed inverters, in particular substitution of (33) in (29), gives

$$\|x_\nu^\star\| \leq \beta_\nu + \gamma_\nu(\|I_{L\nu}\|) + \gamma_\nu\beta_{droop}. \tag{34}$$

Thus, the connection of Fig. 3 is $\mathcal{L}$-stable.

6. NUMERICAL EVALUATION

To validate the stability, performance, and robustness of the PBC operating together with the droop controller, we use a single-phase MG of nine nodes presented in Fig. 4 and taken from (Sauer et al. [2017]). The figure shows three grid-forming inverters controlled by (17), among which the power consumption is distributed. The network parameters are presented in Table 1.

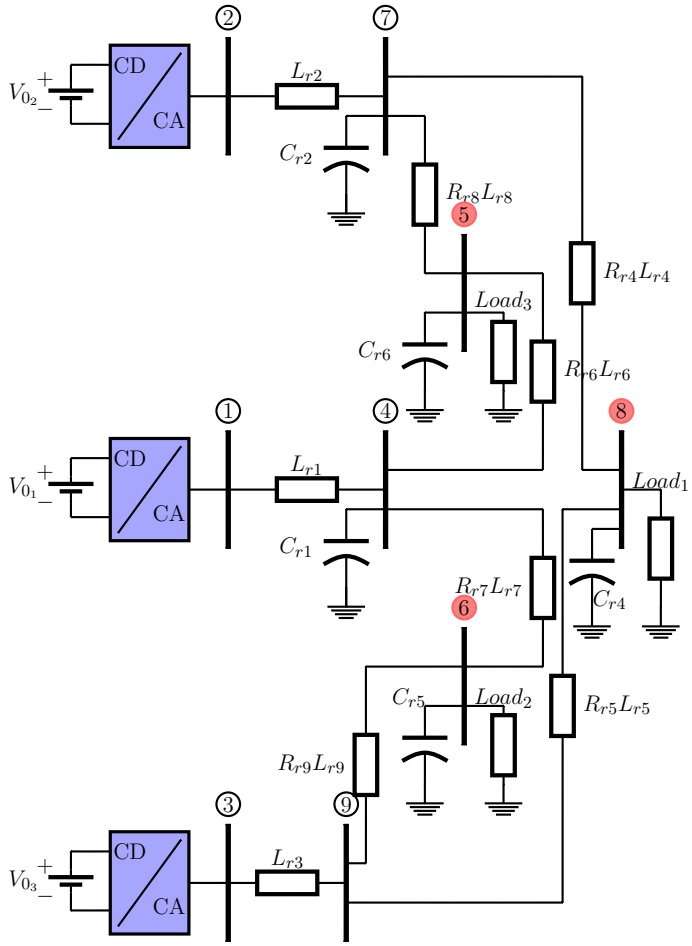

Fig. 4. Single-phase MG with nine nodes, three sources and three loads.

The generation units have the same parameters but we assume that the units have different apparent power capacity. In this sense, each inverter is powered by $V_{0,i} = 400\ V$ DC voltage source, and the power ratings are $S_1 = 20\ kVA$, $S_2 = 10\ kVA$, and $S_3 = 5\ kVA$. The filters' inductors and capacitors are $L_{\nu,i} = 2.35\ mF$ and $C_{\nu,i} = 28\ \mu F$ with parasitic resistances $r_{L,i} = 0.9\ \Omega$ and $r_{C,i} = 100\ M\Omega$, respectively. The droop coefficients are $n_i = \frac{K_e E_{ref}}{4S_i}$ and $m_i = \frac{\omega_{ref}}{10S_i}$, while $K_e = 10$, $E_{ref} = 127\ V_{RMS}$ and $\omega_{ref} = 2\pi f_{ref}$ with $f_{ref} = 60\ Hz$. The parameter $k_E = k_z = 10$ and $c = E_{qi}/2.4E_{ref}^2$, while the controller's gains are $K_{p\nu,i} = 10$ and $k_{i\nu,i} = 1$.

With respect to the power references, the considered profiles are shown in Fig. 5(a) for the grid–forming sources and in Fig. 5(b) for the active power demanded by the loads connected in nodes 5, 6 and 8. The variations in these behaviors emulate the intermittent availability of the generated power for the inverters with some changes in the demand. In time $t = 0$ [s], a load of 6 [kW] is connected in node 8 and a load of 4 [kW] in node 6. Finally, in time $t = 20$ [s], a load of 10[kW] is connected to node 5.

6.1 Simulation results

The numerical evaluation was performed in the Simulink of MATLAB^{TM} with a Runge-Kutta variable step-size integration method. During the first 20 [s], there is only active power demand in nodes 6 and 8; in node 6 the demand is 5 [kW] and 7 [kW] in node 8 such that the total active power demanded is 12 [kW]. The power capacities of the grid-forming inverters satisfy that

$$S_1 = 2S_2 \text{ and } S_2 = 2S_3.$$

Fig.5(a) shows the active power generated by the inverters. Notice that the power of inverter 1 is twice the power supplied by inverter 2 which in turn is twice the power generated by inverter 3, putting in evidence the distribution of the load between the inverters.

In $t = 20$ [s] a load of 9 [kW] is connect to node 5 and it is observed that the distribution of load in the inverters is satisfied, confirming the robustness of the proposed control scheme. Fig. 6(a) shows the reference voltage E_{ref} and the output filter voltages of the inverters. Note that the error in steady state between the reference voltage and the voltages of the inverter, is less than 1.5%, while the maximum error is less than 5% of the nominal value.

To complete the illustration of the stabilization properties of the controller, the reference frequency f_{ref} and the frequency of the inverters are shown in Fig.6(b). Notice that the steady-state error of the frequency of the inverters and the reference frequency are less than 0.03%.

7. CONCLUDING REMARKS

In this paper, it has been shown that the equilibrium point that corresponds to a proper operation of an MG equipped with local PBC controllers and a droop power-sharing scheme is asymptotically stable. The analysis exploited the ISS properties of the closed-loop Hamiltonian system and

Table 1. MG parameters

Element	Value	Element	Value	Element	Value
C_{r_1}	22 μF	L_{r_1}	152 μH	R_{r_1}	–
C_{r_2}	30 μF	L_{r_2}	165 μH	R_{r_2}	–
C_{r_3}	37 μF	L_{r_3}	155 μH	R_{r_3}	–
C_{r_4}	23 μF	L_{r_4}	190 μH	R_{r_4}	0.85 Ω
C_{r_5}	128 μF	L_{r_5}	267 μH	R_{r_5}	1.19 Ω
C_{r_6}	31 μF	L_{r_6}	225 μH	R_{r_6}	0.1 Ω

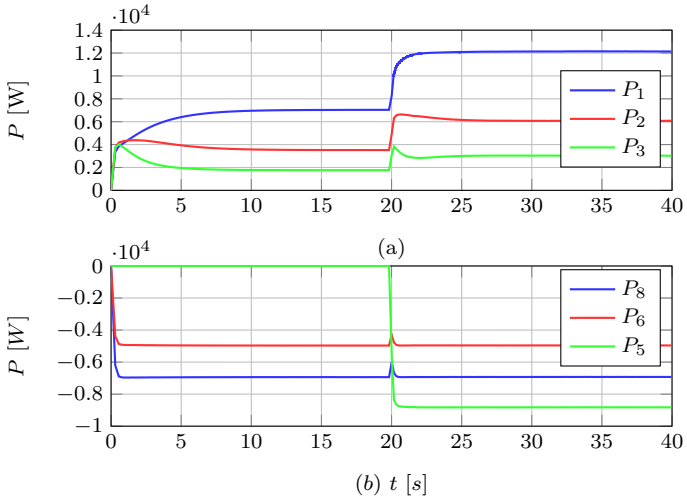

Fig. 5. (a) Active power of the inverters (b) Active power of the load

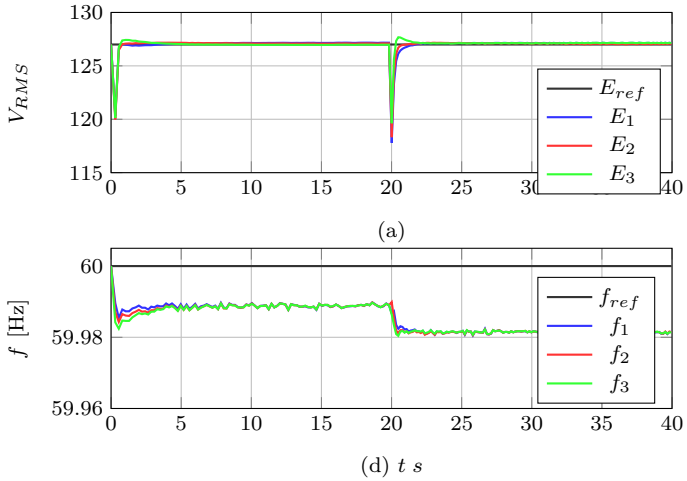

Fig. 6. Voltage and frequency behavior in the output of the inverters.

later on the ISS properties enjoyed by the droop scheme were considered for stating the aforementioned stability result. The validity of the analysis was illustrated via a numerical evaluation.

REFERENCES

Agundis-Tinajero, G., Segundo-Ramirez, J., Visairo-Cruz, N., Savaghebi, M., Guerrero, J.M., and Barocio, E. (2019). Power flow modeling of islanded ac microgrids with hierarchical control. *International Journal of Electrical Power & Energy Systems*, 105, 28–36.

Avila-Becerril, S., Espinosa-Pérez, G., and Canseco-Rodal, R. (2017). On the control of power flows in microgrids. In *Decision and Control (CDC), 2017 IEEE 56th Annual Conference on*, 3252–3257. IEEE.

Avila-Becerril, S., Montoya, O.D., Espinosa-Pérez, G., and Garcés, A. (2018). Control of a detailed model of microgrids from a hamiltonian approach. *IFAC-PapersOnLine*, 51(3), 187–192.

Barklund, E., Pogaku, N., Prodanović, M., Hernandez-Aramburo, C., and Green, T.C. (2008). Energy management in autonomous microgrid using stability-constrained droop control of inverters. *Transactions on Power Electronics, IEEE*, 23(5), 2346–2352.

Cisneros, R., Pirro, M., Bergna, G., Ortega, R., Ippoliti, G., and Molinas, M. (2015). Global tracking passivity-based pi control of bilinear systems: Application to the interleaved boost and modular multilevel converters. *Control Engineering Practice*, 43, 109–119.

Guerrero, J.M., Chandorkar, M., Lee, T.L., and Loh, P.C. (2013). Advanced control architectures for intelligent microgrids, part i: decentralized and hierarchical control. *IEEE Transactions on Industrial Electronics*, 60(4), 1254–1262.

Han, H., Hou, X., Yang, J., Wu, J., Su, M., and Guerrero, J.M. (2016). Review of power sharing control strategies for islanding operation of ac microgrids. *IEEE Transactions on Smart Grid*, 7(1), 200–215.

Khalil, H.K. (1996). Noninear systems. *Prentice-Hall, New Jersey*, 2(5), 5–1.

Konstantopoulos, G.C., Zhong, Q.C., Ren, B., and Krstic, M. (2015). Bounded droop controller for parallel operation of inverters. *Automatica*, 53, 320–328.

Lopes, J., Moreira, C., and Madureira, A. (2006). Defining control strategies for microgrids islanded operation. *Power Systems, IEEE Transactions on*, 21(2), 916–924.

Pedrasa, M.A. and Spooner, T. (2006). A survey of techniques used to control microgrid generation and storage during island operation. In *Proceedings of the 2006 Australasian Universities Power Engineering Conference (AUPEC'06)*, 1–6.

Rajesh, K., Dash, S., Rajagopal, R., and Sridhar, R. (2017). A review on control of ac microgrid. *Renewable and Sustainable Energy Reviews*, 71, 814–819.

Rocabert, J., Luna, A., Blaabjerg, F., and Rodriguez, P. (2012). Control of power converters in ac microgrids. *IEEE transactions on power electronics*, 27(11), 4734–4749.

Rojas, A. and Rousan, T. (2017). Microgrid control strategy: Derived from stakeholder requirements analysis. *IEEE Power and Energy Magazine*, 15(4), 72–79.

Sandoval, G., Miranda, H., Espinosa-Perez, G., and Cardenas, V. (2012). Passivity-based control of an asymmetric nine-level inverter for harmonic current mitigation. *IET Power Electronics*, 5(2), 237–247.

Sauer, P.W., Pai, M., and Chow, J.H. (2017). *Power System Dynamics and Stability: With Synchrophasor Measurement and Power System Toolbox*. John Wiley & Sons.

Schiffer, J., Ortega, R., Astolfi, A., Raisch, J., and Sezi, T. (2014). Conditions for stability of droop-controlled inverter-based microgrids. *Automatica*, 50(10), 2457–2469.

Simpson-Porco, J.W., Dörfler, F., and Bullo, F. (2013). Synchronization and power sharing for droop-controlled inverters in islanded microgrids. *Automatica*, 49(9), 2603–2611.

Tuffner, F.K., Schneider, K.P., Hansen, J., and Elizondo, M.A. (2018). Modeling load dynamics to support resiliency-based operations in low-inertia microgrids. *IEEE Transactions on Smart Grid*, 10(3), 2726–2737.

Zhong, Q.C. and Hornik, T. (2012). *Control of power inverters in renewable energy and smart grid integration*, volume 97. John Wiley & Sons.